THE PERFORMANCE OF STEEL STRUTS IN A BRACED EXCAVATION IN PERTH CBD

Natusha L. Zaremba and Barry M. Lehane
School of Civil & Resource Engineering, The University of Western Australia

ABSTRACT

A deep and wide braced excavation constructed for the new Esplanade Station in the Perth CBD provided a useful opportunity to assess appropriate parameters for retaining wall design by backanalysis of its performance. The section of the wall under consideration involved a staged excavation adjacent to sheet piles supported by three levels of props at the final excavation depth of ~13 m. Two adjacent sheet piles were strain gauged to allow assessment of the wall's bending moment, while the lateral soil movements adjacent to the wall were monitored using inclinometers. The struts were also instrumented with strain gauges and the output from these gauges provides the main focus of this paper. The effects of temperature on the inferred strut loads are examined and it is shown that the data recorded during excavation pause periods could only be explained if the operational axial strut stiffness was about a quarter of its theoretical stiffness. Finite Element backanalyses of the measurements obtained during the excavation phases also show that a best fit between measured and predicted strut loads is achieved for a similar operational stiffness. It is concluded that for large braced excavations of this nature, imperfections/curvatures in long struts lead to strut loads that are significantly lower than expected.

1 INTRODUCTION

A major infrastructural project was recently undertaken by Leighton Kumagai Joint Venture (LKJV) in Perth, Western Australia, to expand the existing rail network by the construction of twin cut and cover and bored tunnels through the heart of the CBD, and two complimentary underground stations. The magnitude and complexity of the works were of an order never before experienced in Perth. The excavation that is considered herein is that of the new Esplanade Station (Figure 1), which was constructed within a 12 m deep excavation retained by temporary sheet piles and multiple propping layers. Unlike many other areas in the CBD, sheet piling at this location was feasible due to the relative remoteness of adjacent structures.

Figure 1: Esplanade Station and cut and cover tunnel works adjacent to the Convention Centre and Swan River.

A large number of struts within the excavations were instrumented throughout the project to check if the excavations were proceeding according to design and, most importantly, as a safety measure for the site personnel working at depth. As described later, axial loads within the struts were measured by averaging the data from four vibrating wire strain gauges attached to each, which in addition to temperature were simultaneously recorded at regular intervals throughout the entire construction period. The extensive monitoring network provided a unique opportunity to investigate the response of these struts in excavations in Perth soils. Temperature variations had a significant effect on the strain gauge output and the (inferred) strut loads and these effects are also examined in this paper.

2 GROUND CONDITIONS

The ground conditions in the area of the Esplanade Station site considered here consist predominantly of fluvial sands, clays and silts - originally referred to as the Guildford Formation and more recently redefined as the Perth Formation (Gozzard, 2007) overlying the Kings Park Formation bedrock. The geotechnical properties of one of the units of the Perth Formation are discussed in Lehane *et al*. (2007). The station was constructed partially through sand fill, which was reclaimed over the past 100 years and believed to have originated from dredged riverbed material removed in the formation of channels within the adjacent Swan River.

The site stratigraphy at the station cross-section examined in this paper is coincident with a comprehensive instrumentation and monitoring array at the centre of the station. The stratigraphy encountered in boreholes and inferred from Cone Penetration Tests (CPTs) at this location is illustrated in Figure 2a. There are slightly different soil conditions on the east and west of the station cross-section, but respective soil layers have been considered to be horizontal in the Finite Element PLAXIS backanalyses discussed later (Figure 2b).

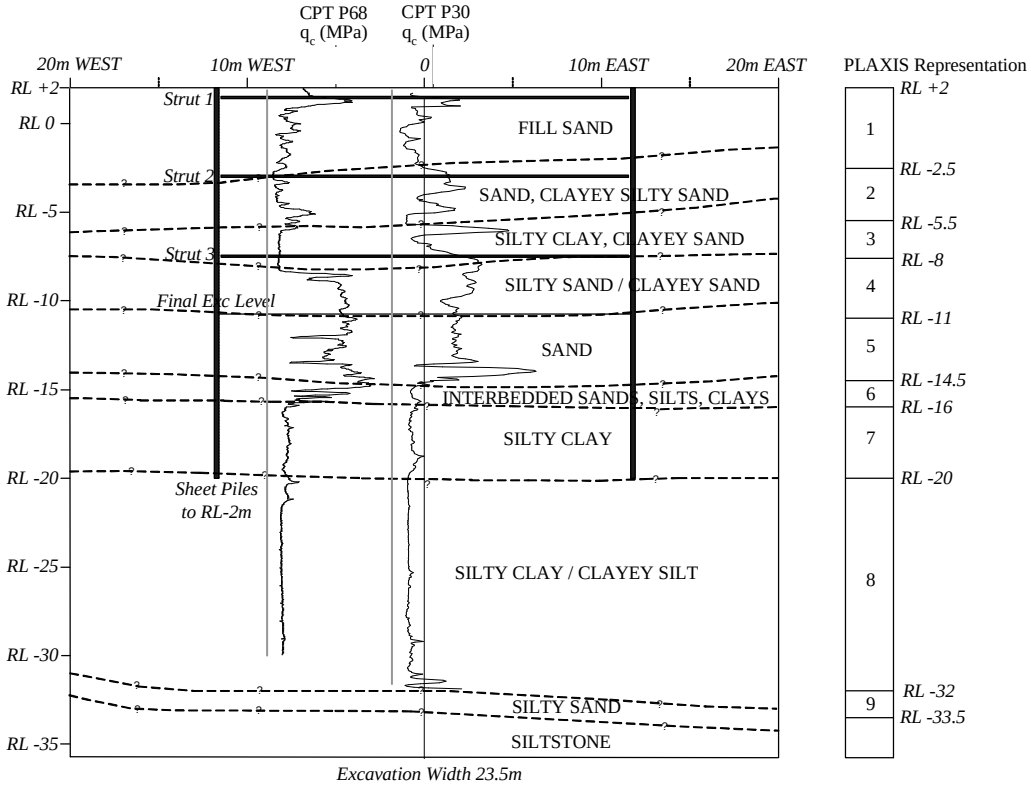

Figure 2: (a) Soil stratigraphy at station cross-section and (b) stratigraphic layers employed in PLAXIS analyses.

The water table was 2 m below the ground surface and therefore dewatering and subsequent recharge outside the retaining structure was an integral part of the construction works. Pre-construction measurements of pore pressures obtained from numerous vibrating wire piezometers installed by LKJV indicate that pore pressures could be assumed to be hydrostatic prior to de-watering.

A simple linear elastic Mohr Coulomb model was adopted for all soils in the PLAXIS analyses described later, each of which was assumed to be fully drained. Based on data presented in Lehane & Fahey (2004) and Lehane *et al*. (2007), the equivalent linear elastic soil moduli of soil layers at the station cross-section were determined using the following relationship between CPT end resistance (q_c) and the vertical effective stress (σ'_v):

$$E_{soil} = \xi \, (q_c^{0.25} \, \sigma'^{0.5}_v \, p_a^{0.25}) \qquad \textbf{(1)}$$

where p_a is atmospheric pressure expressed in the same stress units as q_c and σ'_v
ξ is a constant depending on the strain level.

The selection of parameters for PLAXIS, which are summarised in Table 1, was guided by data presented in Lehane *et al.* (2007) and elsewhere. A ξ value of 100 for use in Equation (1) was adopted above excavation level (where the soil experienced relatively large lateral displacements) while a ξ value of 400 was considered appropriate below the final excavation level (where lateral soil movements were significantly lower). The *in situ* lateral earth pressure coefficients

were assumed to be unity for all soils in the 'Perth Formation' while specified friction angles varied between 30^o and 40^o, depending on the measured fines contents. Permeabilities in the vertical and horizontal direction (k_z and k_x) needed to be specified for the steady state seepage conditions modelled in the PLAXIS analyses; these k_z and k_x values were assessed from the respective particle size distribution curves and a k_x/k_z ratio of 10 was employed for all soils.

Table 1: PLAXIS soil input parameters.

Soil Layer	Description	K_0	E_{soil} (MPa)	Friction Angle (^{o}) with c'=0	k_x (m/s)	k_z (m/s)
1	Sand Fill	0.5	20	35	1×10^{-4}	1×10^{-5}
2	Clayey Silty Sand	1.0	20	30	1×10^{-5}	1×10^{-6}
3	Silty Clay 1	1.0	30	30	1×10^{-8}	1×10^{-9}
4	Sand	1.0	40	40	1×10^{-4}	1×10^{-5}
5	Silty Clay 2	1.0	40	30	1×10^{-8}	1×10^{-9}
6	Silty Sand	1.0	200	40	1×10^{-5}	1×10^{-6}
7	Silty Clay 3	1.0	160	30	1×10^{-8}	1×10^{-9}
8	Clayey Silt / Silty Clay	1.0	180	30	1×10^{-6}	1×10^{-7}
9	Silty Sand	1.0	200	30	1×10^{-6}	1×10^{-7}
	Siltstone	Rigid impermeable				

3 CONSTRUCTION SEQUENCE AND INSTRUMENTATION

3.1 EXCAVATION CONFIGURATION

The sheet piled excavation was retained by three levels of temporary tubular steel struts with a horizontal spacing of 6 m. The excavation was 23.5 m wide (at the cross-section under consideration), and centre vertical support to the struts was provided by connection to kingposts embedded in piles bored to bedrock (Figure 3). Excavation to the final depth of ~13 m was achieved over a period of 6 months. The axial stiffness (EA) of the struts and flexural rigidity (EI) of the sheet piles used are listed in Table 2.

(a)

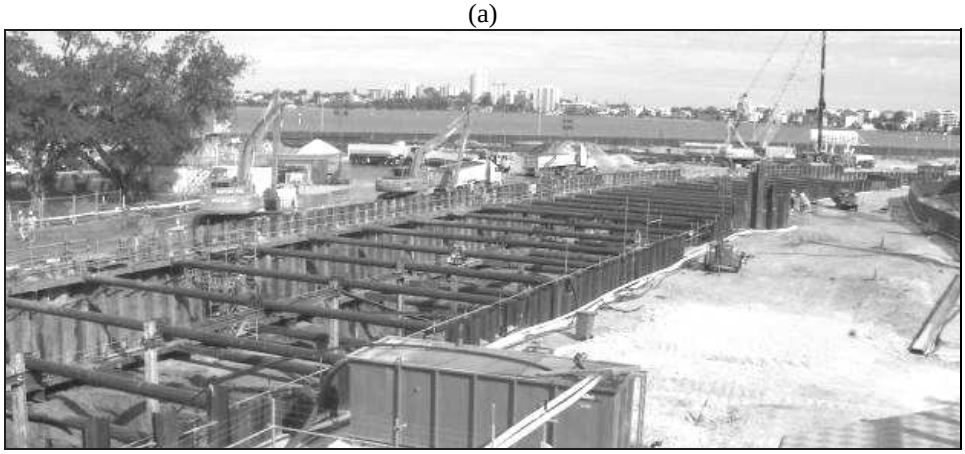

(b)

Figure 3 Photos of the Esplanade Station excavation (a) looking South across the excavation and (b) looking from the West of the excavation

Table 2: Strut and Sheet Pile Details.

Level No.	RL (m)	Depth (m)	Section	Axial Stiffness EA (kN)	EI (kNm^2 / m)
1	+1.5	0.5	CHS 406.6 x 9.5	2.5×10^6	-
2	-3.0	5	CHS 559 x 12.7 with WC400 x 328	5.3×10^6 (Equivalent)	-
3	-7.5	9.5	CHS610 x 9.5	$3.8x\ 10^6$	-
-	-	to 22 m	Sheet Pile PU 24	-	1.1×10^5

3.2 INSTRUMENTATION

Spot weldable vibrating wire strain gauges (Slope Indicator model 52602100; Figure 4a) were used throughout the project to monitor forces in the struts. The struts were instrumented with four gauges at the 3, 6, 9 and 12 o'clock positions at a distance of three times the strut diameter from the end of the strut (Figure 4b). Struts were to be temporarily cast into the permanent structure at the second propping level and therefore at this level (to alleviate the large circular void that a tubular strut would leave upon its removal), 3 m long welded channel (WC) sections were used at the prop ends (see Figure 4c).

The vibrating wire strain gauges (VWSG) recorded strain and temperature simultaneously at 15 minute intervals, providing a detailed record of load change with excavation and also the local load fluctuations induced from diurnal temperature changes. The total axial load in the strut was derived from the average output of the four gauges.

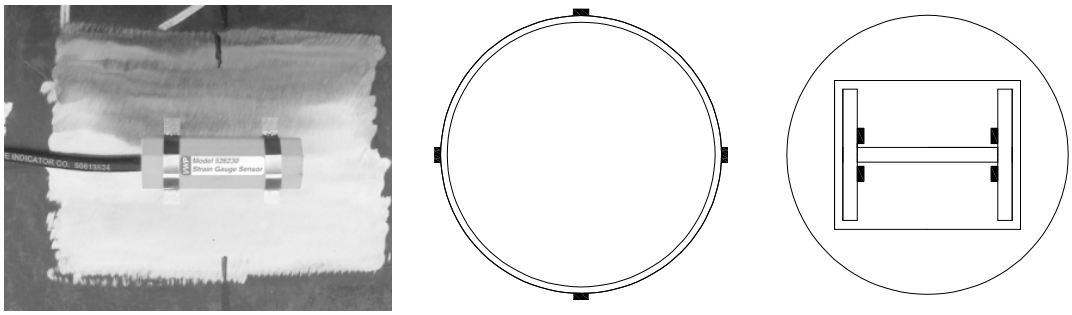

(a) (b) (c)

Figure 4(a): Installed VWSG (b) gauge locations on a tubular prop and (c) welded channel section used at level 2.

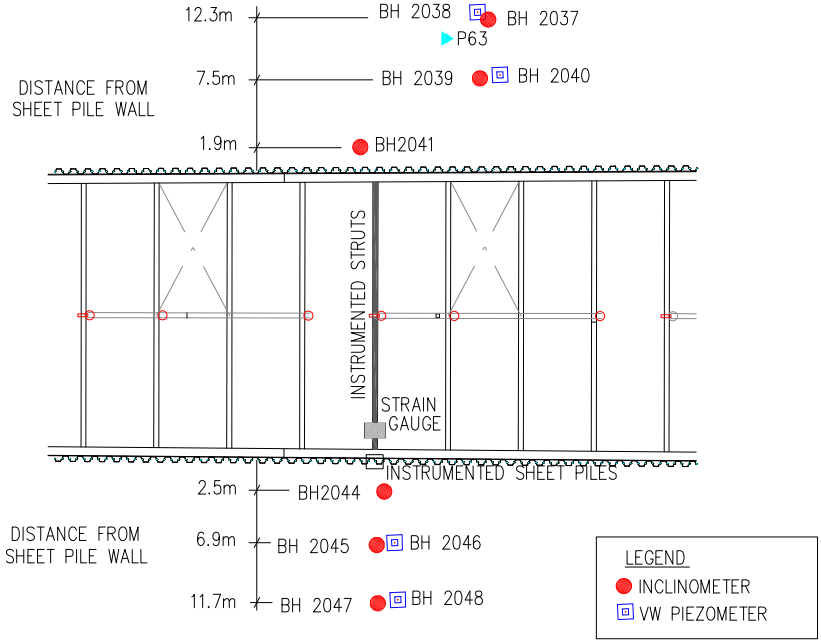

Figure 5: Instrumentation array and strut configuration.

As shown on Figure 5, the cross-section under consideration was coincident with an extensive instrumentation and monitoring array of inclinometers and piezometers. Inclinometers were installed into the Kings Park Formation bedrock typically to depths of 35 to 40 m and these were monitored using a Slope Indicator 0.5 m gauge inclinometer probe and recording unit.

Additional instrumentation in the form of foil resistance strain gauges was installed by UWA on a pair of instrumented sheet piles close to an instrumented set of struts (see Figures 6 and 7). The gauges were installed at 10 separate levels to a depth of 18 m and protected from damage during sheet pile installation by a tack-welded channel section (Figure 7b). At any given level of strain gauges on the wall, it was found that the excavation induced strains on gauges on adjacent sheets were of approximately the same magnitude (±25%) but of opposite sign. This finding indicated that the sheet pile clutches were sufficient to enable the pair of sheets to act as a combined unit and that the relevant sectional modulus for the wall could be assumed to be that of the combined section and not of the individual sheets; the combined EI value is listed in Table 1.

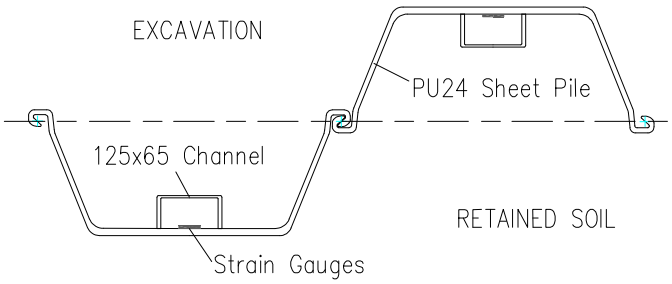

Figure 6: Strain gauge locations on sheet piles.

The bending moment (M) any given strain gauge position could therefore be derived as:

$$M = E\ Z\ \left(|\varepsilon_1| + |\varepsilon_2|\right)/2 \quad \textbf{(2)}$$

where E is the Young's Modulus of steel
Z is the section modulus of the wall (combined sheets)
ε_1 and ε_2 are the changes in strain from the initial zero datum

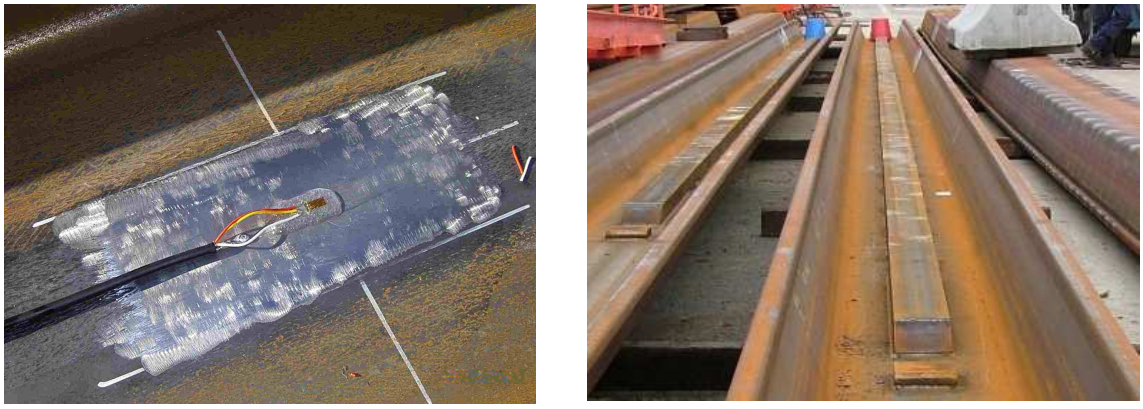

(a) (b)

Figure 7(a): Foil resistance gauge on instrumented sheet pile and (b) completed sheet pile installed with channel section to protect gauges during driving.

The output from the strain gauges varied with temperature and the uppermost gauges also showed fluctuations due to the movement of construction plant. To ensure consistency, strain gauge outputs recorded overnight at a temperature of 15 and 20°C were used for calculation of bendings moments using Equation (2).

LKJV installed a comprehensive array of vibrating wire piezometers (VWPZ) outside the line of sheet piles to monitor the water pressure and to assist in the operation of recharging. These piezometers were usually installed in clusters of three at different depths and indicated an average gradient of pore pressure with of depth of ~8 kN/m^3 during the final stage of excavation; this gradient matched the gradient predicted in the PLAXIS seepage analyses described later.

3.3 CONSTRUCTION SEQUENCE

The station excavation can be considered in terms of four main stages: (1) the installation of the sheet piles and excavation to a depth of 2.0m (Figure 8a), (2) installation of strut level 1 and completion of excavation to 5.7 m depth (Figure 8b), (3) installation of strut level 2 and excavation to 10.5 m depth (Figure 8c) and (4) insertion of strut level 3 and excavation to ~12.5 m depth (Figure 8d). These stages will be referred to in the following presentation of the monitoring data and the stages of analysis.

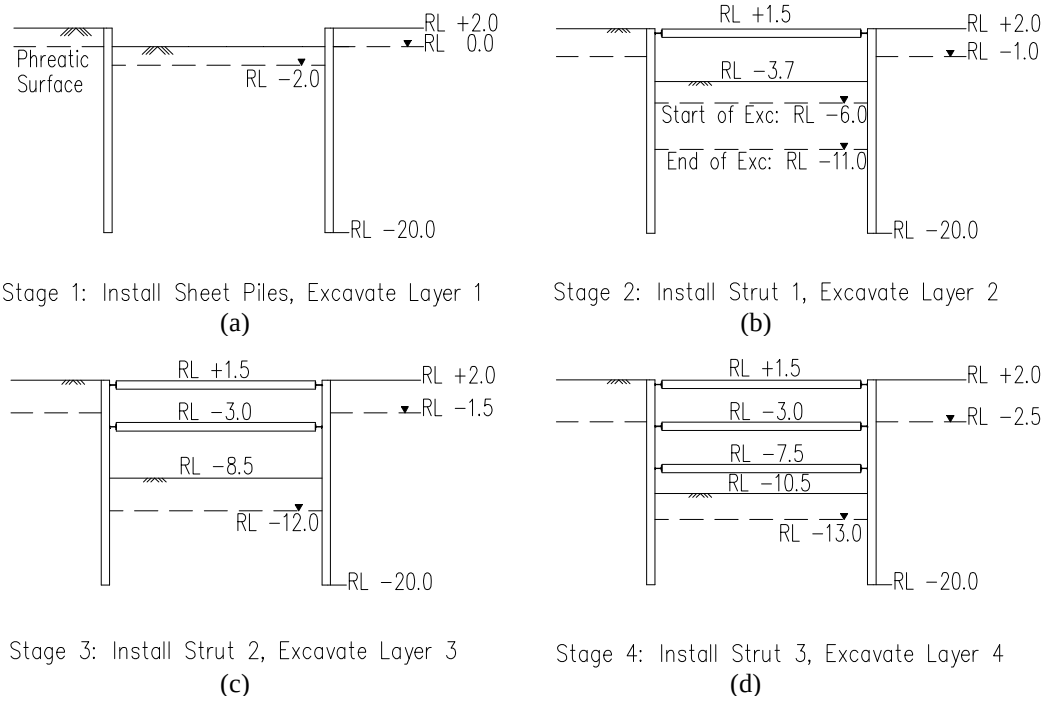

Figure 8: Excavation sequence.

4 EFFECTS OF TEMPERATURE

The strain outputs of the gauges attached to all (free-ended) struts were monitored for a number of days in the LKJV yard on site prior to their use in the excavation works. As both strain and temperature were recorded simultaneously, the specific proportional relationship between temperature induced strain (ε_T) and temperature (T) could be established for each strain gauge and a linear relationship determined with constants m and B:

$$\varepsilon_T = mT + B \quad \textbf{(3)}$$

When installed in the excavation, the compression load measured at each gauge location (F_i) could then be determined (Equation 4) and the force in the strut taken as the average of the forces measured at each of the gauge locations:

$$F_i = -EA(\varepsilon - \varepsilon_T) \quad \text{where EA is the axial rigidity of the strut} \quad \textbf{(4)}$$

It is noteworthy that temperatures varied with location on the struts e.g. the temperature at gauges on the upper exposed surface of the struts during the day was considerably higher than that at the gauges at the underside of struts..

A number of struts were in place for over a year and these experienced a minimum temperature of ~4ºC and maximum temperature of ~56ºC. The maximum mean daily temperature change observed was in the order of 30-35ºC, which has the potential to induce significant temperature loading in the strut. Figure 9 illustrates the variation with temperature of the strut load at level 1, derived using equation (4), during a period of no construction activity (after excavation 2). It is evident that the strut force increases by around 180 kN for a 25°C increase in temperature.

If the installed strut was fully restrained by the waler, wall and soil system, an increase in temperature would result in an increase in strut load of:

$$F_{fixed} = EA\alpha(\Delta T) \quad \textbf{(5)}$$

where F_{fixed} is the force in the fully fixed strut due to a temperature change ΔT
E is the Young's Modulus of steel
A is the cross-sectional area of the steel strut
α is the coefficient of thermal expansion for steel (=1.2x10^{-5}/ºC)

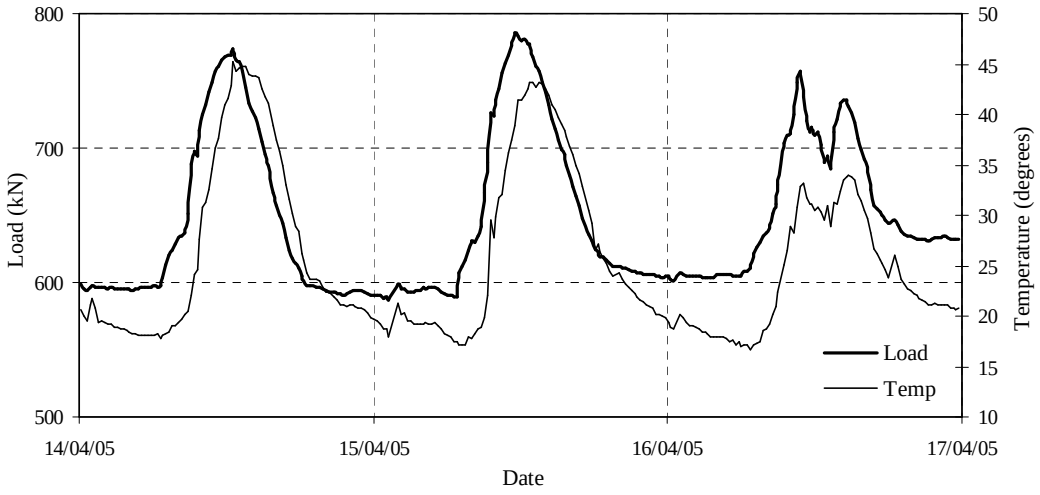

Figure 9: Variation in strut load (Strut 1) with average strut temperature.

Application of Equation (5) to the example shown on Figure 9 indicates that the force in the strut, if its ends were fully restrained, would increase by 750 kN for a temperature increase of 25°C. The observed increases in load are, however, only about a quarter of this value primarily due to the finite stiffness of the soil and any other slack between the waler and sheet pile. Twine and Roscoe (1997) report that for strutted excavations with flexible retaining walls, struts loads were typically between 10 and 25% of F_{fixed} (and up to 40% of F_{fixed} in one case); these proportions are compatible with the example shown in Figure 9. It is therefore clear that, as fully fixed conditions do not operate, the soil behind retaining walls supported by struts is subjected to continuous cycling due to temperature changes. This cycling could lead to shakedown settlements in sand and undrained strength reductions in clays.

If a "lack-of-fit" condition does not exist, the response of the strut and retaining system can be idealised as two linear elastic springs in series. The force induced in the strut due to a temperature change (F_{st}) can be simply expressed in terms of the stiffness of the strut (k_{strut}), a spring constant representing the stiffness of the soil (k_{soil}), the displacement/extension of the strut due to a temperature change in the unrestrained (free) condition (δ_{temp}) and the displacement relief provided by the soil (δ_{soil}) according to:

$$F_{st} = k_{strut}\left(\delta_{temp} - \delta_{soil}\right) = k_{soil}\delta_{soil} \quad \textbf{(6a)}$$

which, when re-arranged, gives:

$$\delta_{soil} = \left[\frac{k_{strut}}{k_{soil} + k_{strut}}\right]\delta_{temp} \quad \textbf{(6b)}$$

where k_{strut} is the spring stiffness of the strut per unit width, $k_{strut} = \dfrac{EA}{(L/2)\,s}$ **(6c)**

L is the length of the strut (=excavation width)
s is the horizontal spacing of struts within the excavation

Equations (6a) may therefore also be expressed as follows to determine the temperature induced load in a strut:

$$F_{st} = \left[\frac{k_{strut}\,k_{soil}}{k_{strut} + k_{soil}}\right]\delta_{temp} \quad \textbf{(6d)}$$

k_{soil} is an equivalent elastic spring stiffness of the soil and its relationship with an equivalent linear elastic Young's modulus for the soil (E_{soil}) was investigated in a series of plane strain Finite Element (FE) analyses of the excavation at the Esplanade. This analysis was conducted using the Oasys SAFE FE package (Oasys, 2003) and examined the effects of a temperature change applied to one individual strut level or to a number of strut levels. For this exercise, the soil was assumed to be a linear elastic material (defined by E_{soil} and Poissons ratio, ν=0.3) and struts were represented as 0.5m thick elastic slabs with a range of axial rigidities, including the rigidities (per metre width) representative of the actual struts used at the Esplanade. A temperature increase was modelled by applying an internal pressure to all the strut elements that resulted in an axial strain of $\alpha\,\Delta T$ in the free condition.

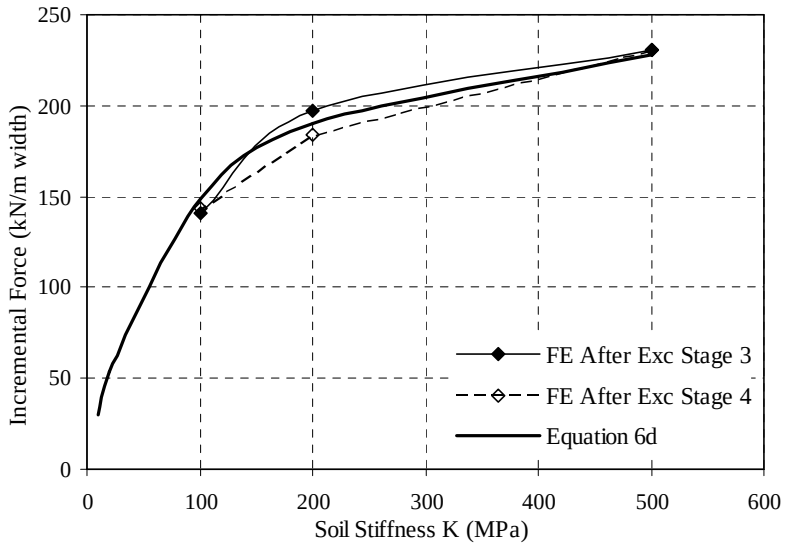

Figure 10: Comparison of strut load for Strut 2 from finite element analysis, 25° temperature change ($k_{soil}=E_{soil}$ per unit width).

Although different relationships between k_{soil} and E_{soil} were examined, best agreement between Equation (6d) and the FE predictions was obtained when k_{soil} (per unit width) was simply assumed equal to E_{soil}. Figure 10 provides an illustration of this agreement for the case of the mid-level strut (Strut 2). Good agreement adopting $k_{soil}=E_{soil}$ was also evident for strut level 3 but a best-fit k_{soil}/E_{soil} ratio of ~0.75 was obtained for strut level 1, reflecting the influence of the free surface.

The following equation may therefore be used to predict the temperature induced load, per unit width, in a deep strut (F_{st}) - noting that k_{strut} is the strut spring stiffness per unit width:

$$F_{st} = \left[\frac{k_{strut}\ E_{soil}}{k_{strut} + E_{soil}}\right]\delta_{temp} = \left[\frac{k_{strut}\ E_{soil}}{k_{strut} + E_{soil}}\right]\alpha L\,\Delta T \qquad \textbf{(7)}$$

There were many instances over the course of the excavation for the Esplanade station when changes in strut loads due to temperature changes alone could be deduced. These data were compiled for the three strut levels and it was immediately apparent that the temperature induced loads could only be predicted using Equation (7) when the equivalent soil modulus (E_{soil}) was considerably lower than could reasonably be expected e.g. see stiffness data for the Perth Formation presented in Lehane *et al.* (2007). Moreover, PLAXIS backanalyses for the excavation (discussed later) and other backanalyses performed using the Oasys FREW program (Smith, 2007) indicate that excavation induced strut loads are over-predicted significantly. This observation combined with the incompatibility of Equation (7) with measured temperature loads indicate that operational axial strut stiffness ($k_{strut\text{-}op}$) is well below the theoretical value given in Equation (2c). The operational strut stiffness ($k_{strut\text{-}op}$) may therefore be expressed as:

$$k_{strut\text{-}op} = \mu\ k_{strut} \text{ where } \mu<1 \qquad \textbf{(8)}$$

Calculations to assess the strut efficiency (μ) were performed using F_{st} values measured at strut levels 2 and 3 and by backfiguring an E_{soil} value to achieve compatibility with Equation (7).

E_{soil} may be assumed to vary approximately with the CPT end resistance (q_c) and the vertical effective stress in the vicinity of the strut (σ'_v) according to Equation (1). The values of E_{soil} backfigured using Equation 7 and hence the ξ values as well as the δ_{soil} values are plotted on Figure 11 for a range of strut efficiency factors (μ). It is apparent that E_{soil} and ξ values depend strongly on the assumed μ value.

The cyclic nature of temperature loading combined with the relatively low levels of soil displacement induced by this loading are such that the value of ξ for use in Equations (1) and (7) should correspond to that of an equivalent elastic unload-reload value at low strains (which differs from that operational during the staged excavation). Based on the proposals of Lehane *et al.* (2007), it may therefore be expected that the value of ξ is at least 200 – which Figure 11b indicates is consistent with a strut efficiency (μ) of about 0.25 to 0.3. The calculated soil displacements corresponding to ξ =200 range from 0.3 mm to 0.6 mm (which represent less than 25% of the free thermal strut expansion) suggest low thermal-induced cyclic strains and an even higher ξ value and low μ value. It follows that the strut efficiency (μ) is of the order of 25% and could be even lower. 'Lack-of-fit' effects are unlikely to be significant for the temperature case examined here (when struts are already under high compression loads). Zaremba (2008) will show that the low values

of μ may be explained by effects of initial curvature as well as curvature due to self-weight deflection and differential temperature.

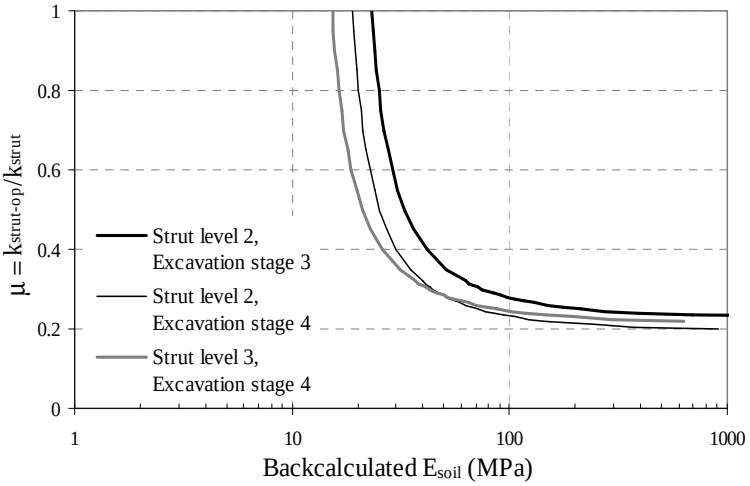

(a)

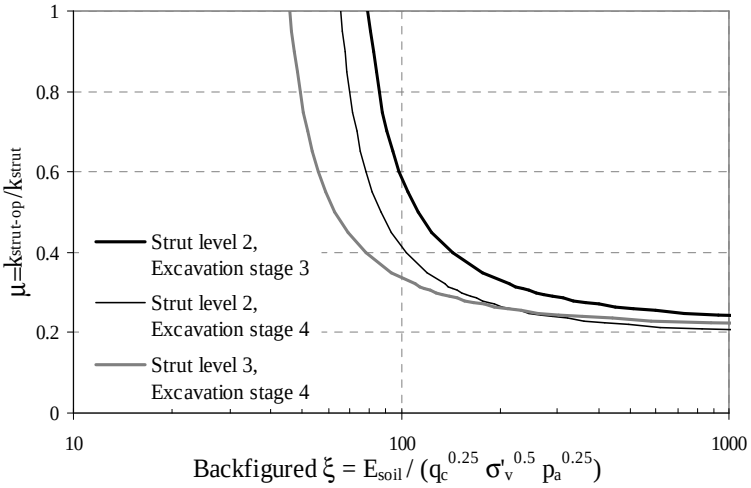

(b)

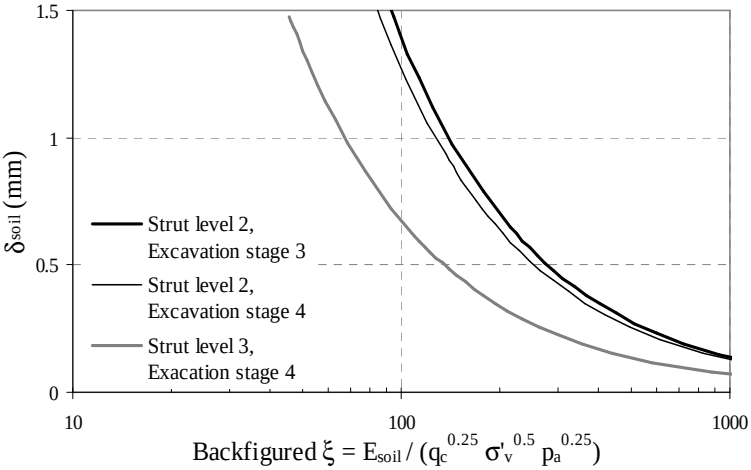

(c)

Figure 11: Backfigured values of E_{soil}, ξ and δ_{soil} for a range of strut efficiency factors (μ).

5 BACKANALYSIS

PLAXIS was used to model the excavation sequence to final excavation level. Figure 12 illustrates the PLAXIS 2D plane strain mesh employed and the corresponding soil input parameters are listed in Table 1. The wall was modelled as a series of beam elements with a soil-wall interface friction angle of 0.66 times the soil friction angle (φ'). The struts were modelled as elastic springs (per metre run) and the initial analysis performed assumed a strut efficiency (μ) of 1. The seepage analyses for each stage modelled by Plaxis predicted pore pressures consistent with those measured by the vibrating wire piezometer records; see Section 3.3.

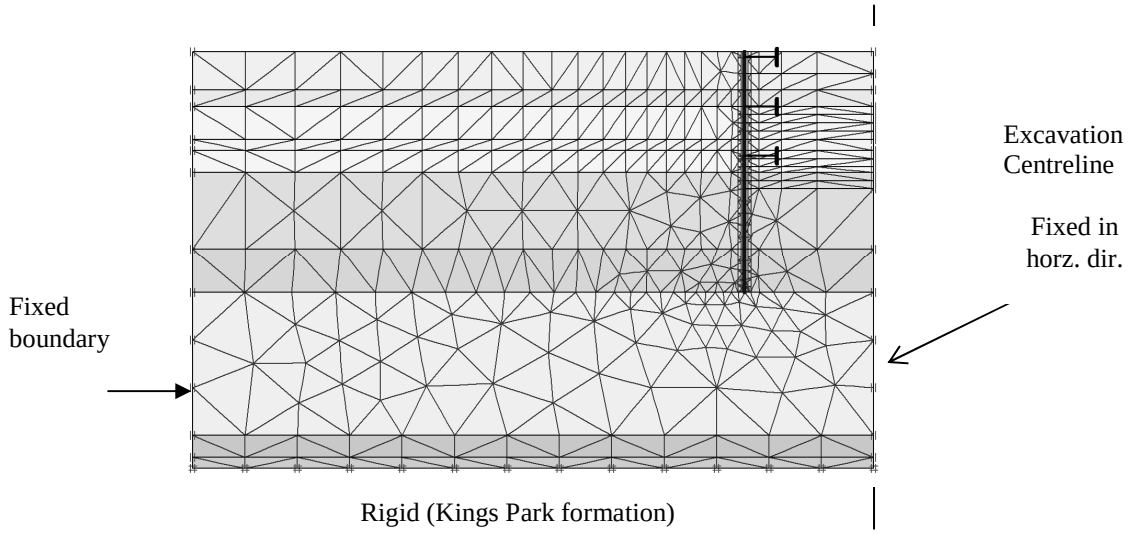

Figure 12 PLAXIS plane strain mesh

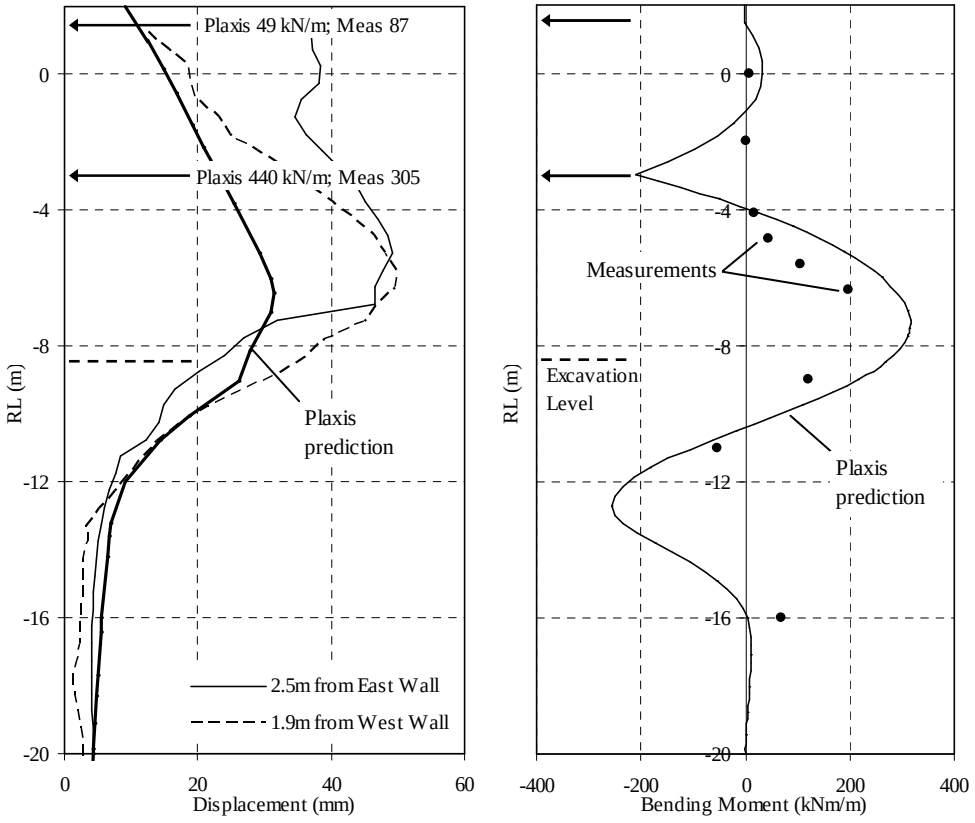

(a) (b)

Figure 13(a): Measured displacements and strut forces and (b) bending moments compared with PLAXIS results for a strut efficiency (μ) of unity.

The initial analysis of all excavation stages using $\mu = 1$ showed that soil movements at inclinometer locations were under-predicted and strut loads are over-predicted. Predictions for Stage 3 (which involves excavation to layer 3; see Figure 8) are compared with measurements in Figure 13. It is evident that maximum lateral displacements are under-predicted by almost a factor of two while the strut force at level 2 is over-predicted by 50%.

In keeping with the observations made in Section 4, a second analysis was performed using a strut efficiency factor (μ) of 0.2 with all other parameters remaining identical. Figure 14 presents a comparison of measurements and PLAXIS predictions for Stage 3 for this case. It is apparent that the use of a reduced strut stiffness leads to improved predictions for maximum lateral movement and the strut force at levels 1 and 2. This finding combined with the inferences made regarding temperature induced strut forces (Section 4) indicates that the operational stiffness of struts was only 20% of their theoretical values.

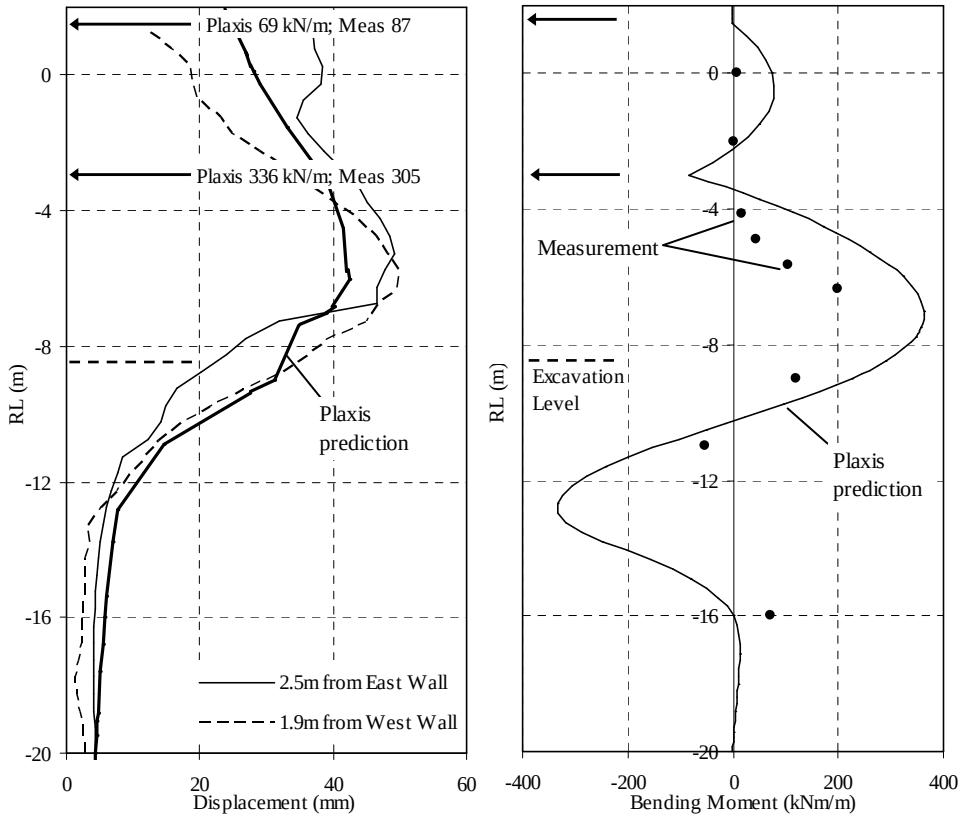

Figure 14 (a) Measured displacements and strut forces and (b) bending moments compared with PLAXIS results for a strut efficiency (μ) of 0.2.

As seen on Figure 14, both displacements and bending moments are relatively well predicted (although slightly better predictions of bending moment are seen in Figure 13). Unfortunately, malfunctioning strain gauges located at about RL -14m did not permit comparison of the observed negative bending moments around this level.

6 CONCLUSIONS

This paper describes the performance of steel struts in a braced excavation in the Perth CBD. It was observed that:

1. The vibrating wire strain gauges employed provide a reliable and accurate means of measuring strut loads. The simultaneous measurement of strain and temperature allowed diurnal temperature effects in the struts to be identified and assessed.
2. Excavation induced strut loads are over-predicted significantly and displacements are under-predicted if the axial stiffness of struts is taken as equivalent to the theoretical value for straight structural members. The operational axial stiffness of the steel tubular struts used at the Esplanade was only 20% of the theoretical value; such a low efficiency can be explained by a relatively modest initial curvature in long struts.

3. The operational equivalent elastic soil stiffness (E_{soil}) adjacent to the sheet piles at the Esplanade may be expressed using Equation 1 [$E_{soil}= \xi (q_c^{0.25} \sigma'_v{}^{0.5} p_a^{0.25})$], where ξ =100 above excavation level for the observed maximum lateral movement of ~50 mm; higher values of ξ operate at lower strain levels.

7 ACKNOWLEDGEMENTS

The authors gratefully acknowledge the funding provided by an Australian Research Council (ARC) linkage grant in association with Leighton Kumagai Joint Venture (LKJV). The assistance provided by all staff at LKJV is very much appreciated.

8 REFERENCES

Gozzard B. (2007). A reinterpretation of the Guildford Formation. *Australian Geomechanics*, 42(3) (This issue).

Lehane B.M., Mathew G. and Stewart D. (2007). A laboratory investigation of the clay and silt in the upper horizons of the Perth/Guildford Formation in the Perth CBD. *Australian Geomechanics*, 42(3). (This issue)

Lehane B.M. and Fahey M. (2004). Using SCPT and DMT data for settlement prediction in sand. *Proc. 2nd International Conf. on site characterisation*, Porto, Portugal, 2, 1673-1680.

Oasys (2003). Oasys manual for SAFE. Ove Arup & Partners, London W1P 6BQ.

Smith M. (2007). Back-analysis of the performance of braced excavations in the Perth CBD. Honours thesis, University of Western Australia

Twine D. and Roscoe H. (1997). Prop loads: guidance on design, CIRIA Core Programme Funder's Report FR/CP/48. London: Construction Industry Research and Information Association.

Zaremba N.L. (2008). Soil-structure interaction effects due to excavation and EPB tunnelling in alluvial deposits. PhD thesis, University of Western Australia (in preparation)